An Efficient Solution Technique for the Simulation of Nonisothermal Multiphase Multicomponent Processes in Porous Media

H. Class[1], R. Helmig[1], P. Bastian[2]

[1] *Institut für Wasserbau*
Chair for Hydromechanics and Modeling of Hydrosystems
University of Stuttgart, Germany

[2] *Interdisziplinäres Zentrum für wissenschaftliches Rechnen*
University of Heidelberg, Germany

Abstract

1 Introduction

Multiphase multicomponent models for the simulation of processes in the subsurface are widely used in different fields of technical application. Characteristic for such models is that they consider flow of more than one fluid phase (e.g., water, oil, gas, alcohol) and transport of components in the fluid phases. Many multiphase multicomponent processes are strongly affected by nonisothermal effects, in particular when processes like evaporation/condensation play a dominant role. Since the 1970s numerical models are developed in the petroleum industry (e.g., Aziz and Settari, 1979 [3]; Aziz et al, 1987 [2]; Coats et al., 1976 [17]; Coats, 1974 [16]), e.g., in order to help optimizing tertiary oil production by steam flooding. In environmental engineering since the 1980s an increasing number of problem tasks shows needs of numerical simulations (e.g., Bear, 1972 [8]; Looney and Falta, 2000 [33]; Helmig, 1997 [25]; Kueper and Frind, 1990 [29]; Panday et al., 1995 [34]), mainly motivated from groundwater protection or groundwater management.

For the description of temperature dependent processes, in addition to a consideration of the flow of the individual phases, transitions of components between the phases, coupled with an exchange of thermal energy, have to be taken into account. Temperature dependent multiphase multicomponent flow and transport processes are given, e.g., during thermally enhanced remediation of contaminated sites. In PAPER II a more detailed description of thermally enhanced soil vapor extraction is given. This technique represents a potentially effective means for in-situ remediation of soils contaminated by nonaqueous-phase liquids (NAPLs) such as halogenated organic solvents or hydrocarbon fuels (e.g., Udell and Stewart, 1989 [43]; Betz et al., 1998 [9]; Class, 1999 [14]). Another risk for groundwater contamination arises from leaking disposal sites. E.g., the clay sealing at the bottom of municipial landfills may dry up such that cracks can

develop, through which leachate may seep. The drying processes are caused by high temperatures inside the landfill as a result of microbiological decomposition. Modeling these processes therefore requires a multiphase multicomponent model concept as well (Bielinski, 2001 [10]). The production of steam in geothermal reservoirs (e.g., Pruess and Narasimhan, 1982 [39]) or in the near-field of nuclear waste disposals (e.g., Bastian et al., 2000 [6]) is also an important task for the application of nonisothermal multiphase multicomponent models.

Sophisticated numerical modeling capabilities are needed to simulate such complex physical processes. In recent years several models have been developed for simulating multiphase flow in porous media. Still only a few of them take into account nonisothermal processes including mass transfer between the phases. Based on a control volume finite element method, Forsyth (1993) [22] developed a model for simulating steam flushing for DNAPL-contaminated sites. Well known in the literature is the multiphase multicomponent simulator TOUGH2 (Pruess, 1987 [37]; Pruess, 1991 [38]). This code uses an integral finite difference method. TOUGH2 also builds the basis for some further developments, e.g., a code for the simulation of steam injection into NAPL contaminated soils by Falta et al. (1995) [19], or a model for simulating the transport of multiple organic components by Adenakan et al. (1993) [1]. Still, the validation of all these models using measurements or experimental data is incomplete and therefore a field of intensive research. Emmert (1997) [18] was able to identify individual processes and to reproduce experimental data for steam injection in a laboratory sand column. He used a nonisothermal twophase twocomponent model, which was based on the multiphase simulator MUFTE (Helmig et al, 1996 [26]; Helmig, 1993 [24]).

With the physics described by the multiphase multicomponent models getting increasingly complex, this yields large systems of coupled partial differential equations with large numbers of unknowns. Thus, the development of fast and efficient solution methods becomes an important or even essential task in order to reduce computing time. Parallelization strategies and improved iterative solution and discretization methods are possible options to achieve this goal. A good survey of the current state of the art in this field give Bastian (1999) [5] and Helmig (1997) [25]. Bastian and Helmig (1999) [7] describe the application of a multigrid preconditioner as an efficient strategy for the solution of the fully coupled twophase flow equations. They used the program system MUFTE_UG (Helmig et al., 1998 [27]), which is designed as a research code to combine the modeling of the relevant physical processes with the application of new discretization techniques and solution methods along with, e.g., multigrid and parallelization strategies.

The intention of this work covers different tasks. First, a sophisticated physical model concept was elaborated that allows the description of nonisothermal multiphase multicomponent systems with variable phase states (see Section 2). Therefore we developed an algorithm that is capable of an adaptive switching of the primary variables according to the local phase state. Then, we extended the multigrid method implemented in the numerical simulator MUFTE_UG in

order to allow its application together with the primary variable substitution algorithm. Within this paper, the physical and thermodynamical model concept for a nonisothermal threephase threecomponent system including the fluid phases water, NAPL, and gas, the concept of primary variable switching, as well as the therefore necessary extension of the multigrid method are explained in detail (Sections 2, 3, and 4). At the end of this paper, an example is given that shows the performance of the extended multigrid preconditioner (Section 5). The physical problems, on which we focus our interest of modeling, deal mainly with the remediation of NAPL contaminated sands by injection of steam or steam-air mixture and simultaneous extraction of the gas phase. This is the motivation for a further important part of our work, which is the validation of the model by means of experimental data, presented in PAPER II. Therefore we used a laboratory experiment with a NAPL contaminated sand column that was cleaned up by a steam injection and monitored by temperature measurements. Further we present a numerical study of different remediation scenarios by isothermal and thermally enhanced soil vapor extraction in a two-dimensional container. Thereby, the fundamental processes affecting the success of the chosen remediation method can be identified, which enables to use the simulator for supporting optimization strategies in practical applications.

2 Physical and Thermodynamical Model Concept

The formulation of a mathematical/numerical model requires an idealization of the physical processes in a way that the natural systems are simplified but at the same time the characteristic properties of the processes in a system be maintained. In this section, we present the model concept we use for the simulation of nonisothermal water–gas–NAPL systems at low pressures (in the magnitude of the atmospheric pressure). The considered temperature range reaches up to 200°C (473 K). We start with clarifying some terms, definitions, and assumptions.

Phases and components: The term 'phase' describes matter that has a homogeneous chemical composition and physical state. Solid, liquid, and gaseous phases can be distinguished. While there can be several liquid phases present in a porous medium, only one gas phase can exist. The phases are separated from each other. The term 'component' stands for constituents of the phases, which can be associated with a unique chemical species. In this work we consider air simplifying as a single pseudo-component and neglect its composition of N_2, O_2, and CO_2. We assume that our water–gas–NAPL systems be composed of the phases water (Subscript w), gas (g), and NAPL (n). These are composed of the components water (Superscript w), air (a), and the organic contaminant (c) (see Fig. 1).

Thermal, chemical, and mechanical equilibrium: For the considered nonisothermal multiphase processes in porous media we state that the assumption of local thermal equilibrium is valid since flow velocities are small. We neglect chemical reactions and biological decomposition

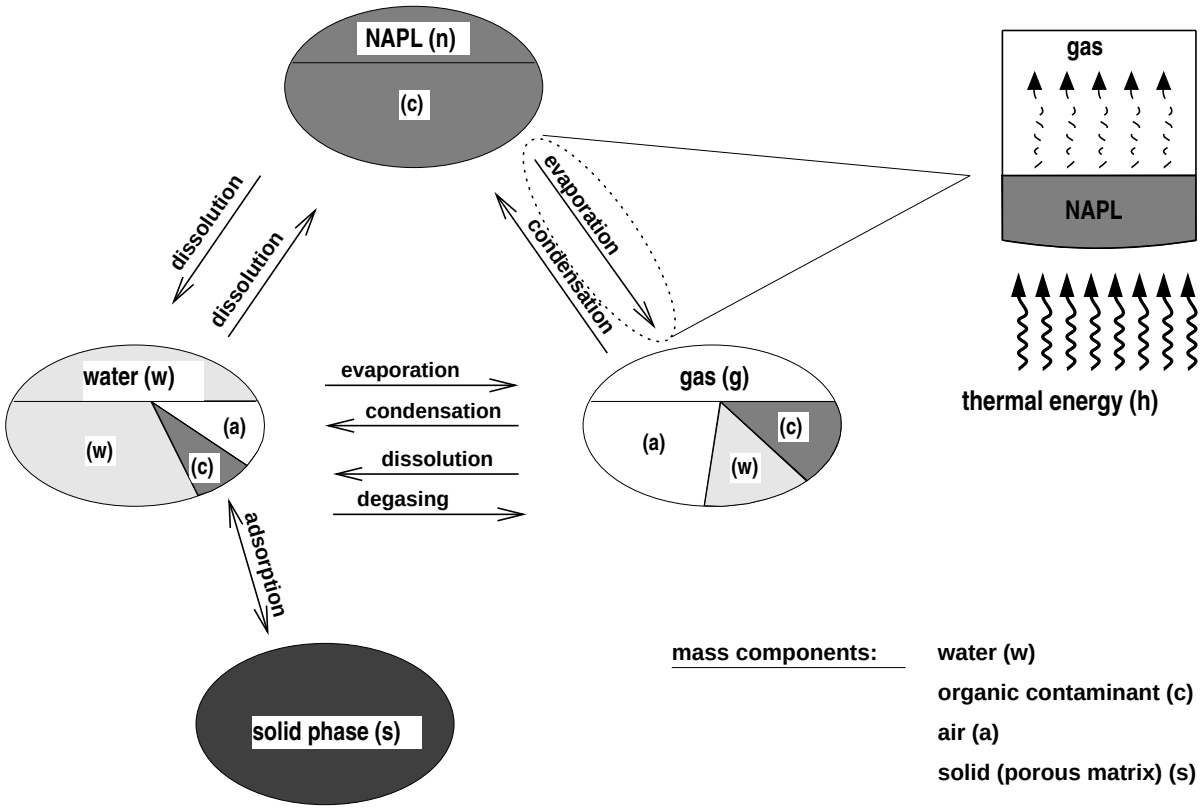

Figure 1: Mass and energy transfer between the phases

and assume chemical equilibrium. Mechanical equilibrium is not valid in a porous medium since discontinuities in pressure can occur across a fluid-fluid interface due to capillary effects.

Phase states and mass transfer between phases: The number of phases existing in a given control volume is not necessarily constant. The 'phase state' indicates which phases are locally present in the control volume (Tab. 2). Displacement processes or mass transfer between the phases may cause appearance or disappearance of fluid phases. Mass transfer processes which we take into account in our model concept are dissolution, degasing, evaporation, condensation, and in some cases also adsorption (Bielinski, 2000 [10]). As a simplification we say that the NAPL phase contains no dissolved components (Fig. 1). For the water phase we assume that the concentrations of the dissolved components air and organic contaminant are low. Thus, dissolution can be described by Henry's Law. Evaporation and condensation allow mass transfer between the phases water and gas or NAPL and gas respectively. This kind of processes is strongly coupled with an exchange of thermal energy, at which the latent heat of vaporization for the water component ($\approx$ 2258 kJ/kg at 100°C, 1 bar) is about a factor of 5 higher than for the NAPL (organic contaminant).

In the following the functions and simplifications used for the computation of secondary variables are given. Their functional dependence on the primary variables is summarized in Tab. 1. Note

that some variables may represent secondary or primary variables dependent on the phase state (Section 3).

2.1 Mole Fractions

The composition of a phase α of the components K is expressed by mole fractions x_α^K with the supplementary constraint

$$\sum_K x_\alpha^K = 1\,. \tag{1}$$

We compute the mole fractions of water and organic contaminant in the gas phase by

$$x_g^K = \frac{p_g^K}{p_g}\,, \qquad K \in \{w, c\}\,. \tag{2}$$

Then the air mole fraction in the gas phase is obtained by $x_g^a = 1 - x_g^w - x_g^c$. For applying Eq. (2), we use Dalton's Law

$$p_g = \sum_K p_g^K \tag{3}$$

and assume validity of the Ideal Gas Law for all components in the gas phase:

$$p = \frac{n\,RT}{V} \tag{4}$$

Here, $R = 8.314\mathrm{J/(mol\ K)}$ is the universal gas constant, n represents the quantity of the gas in [mole], and V in [m^3] is the volume occupied by n. The partial pressure p_g^K of the components water and organic contaminant in the gas phase is equal to the saturation pressure (Fig. 2), presuming that the corresponding liquid phase is present. Otherwise the respective mole fraction in the gas phase is treated as a primary variable (see Section 3). We compute mole fractions of air and organic contaminant in the water phase by using Henry's Law

$$x_w^K = \frac{p_g^K}{H_w^K}\,, \qquad K \in \{a, c\}\,, \tag{5}$$

where H_w^K is the Henry–coefficient. Then, analogously to the air component in the gas phase, we get $x_w^w = 1 - x_w^a - x_w^c$.

2.2 Density

For the computation of the densities of the liquid phases, pressure effects are neglected, whereas the gas phase density is strongly dependent on pressure and temperature. Transforming Eq. (4) yields the molar density $\varrho_{mol,g}$ of the gas phase

$$\varrho_{mol,g} = \frac{n}{V} = \frac{p_g}{RT}\,. \tag{6}$$

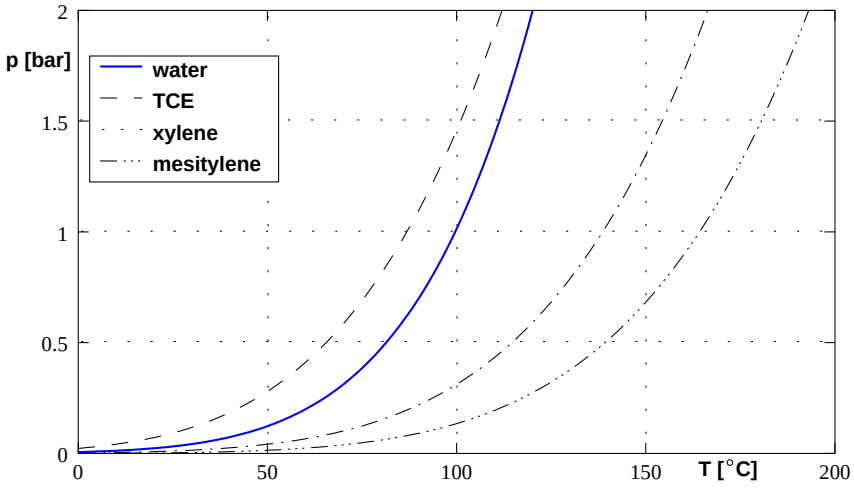

Figure 2: Saturation pressure curves of water and some NAPLs

The molar density of the water phase can be taken, e.g., from International Formulation Committee (IFC, 1967) [28] and an estimation for the NAPL molar density is given, e.g., in Lide and Kehiaian (1994) [32] or Reid et al. (1987) [40]. The mass density of a phase α is obtained by

$$\varrho_{mass,\alpha} = \varrho_{mol,\alpha} \cdot \sum_K x_\alpha^K M^K \,, \tag{7}$$

where M^K represents the molecular weight of component K.

2.3 Viscosity

The dynamic viscosity of the gas phase is dependent on composition. For its computation, we use the Wilke method (Reid et al., 1987) [40]. Approaches for the NAPL phase viscosity as a function of temperature can also be found in Reid et al. (1987) and for the water phase by the IFC (1967) [28].

2.4 Specific Internal Energy and Specific Enthalpy

Since we have to formulate an energy balance equation, we need to determine the caloric state variables of a thermodynamic system, namely the specific internal energy u_α and the specific enthalpy h_α of the fluid phases. u_α stands for the total energy of the molecules of phase α per mass unit (kg). The derivation of the specific internal energy with respect to temperature gives the specific heat capacity at constant volume. If the volume is not constant, the amount of thermal energy brought into a system does not equal the variation of internal energy. The difference can be expressed by the product pv and represents the volume changing work. The

specific enthalpy is then given by

$$h_\alpha = u_\alpha + p_\alpha v_\alpha = u_\alpha + \frac{p_\alpha}{\varrho_{mass,\alpha}} \tag{8}$$

While for the liquid phases water and NAPL the volume changing work can be neglected ($u \approx h$), it has to be taken into account for the compressible gas phase. The specific enthalpy of water and water vapor can be taken from tables of IFC (1967) [28], while Reid et al. (1987) [40] give approximations of specific enthalpies for a large number of organic liquids (NAPLs) and their corresponding vapors.

2.5 Heat Conductivity

Since the assumption of a local thermal equilibrium is made, the heat conductivity of the fluid-filled porous medium (λ_{pm}) is averaged from the heat conductivities of the phases and the solid matrix (e.g., Somerton et al., 1974). For the three phase system water–NAPL–gas we modified the Somerton approach to:

$$\lambda_{pm} = \lambda_{pm}^{S_w=S_n=0} + \sqrt{S_w}(\lambda_{pm}^{S_w=1} - \lambda_{pm}^{S_w=0}) + \sqrt{S_n}(\lambda_{pm}^{S_n=1} - \lambda_{pm}^{S_n=0}) \tag{9}$$

2.6 Diffusivity

The term 'hydrodynamic dispersion' merges two different physical effects, namely molecular diffusion, which is caused by the motion of the molecules, and mechanical dispersion, which describes the transport of components due to fluctuations of the velocity on the pore scale. With phase velocities getting smaller the quota of molecular diffusion increases. In our model we neglect mechanical dispersion and consider only molecular diffusion in the gas phase. Normally, molecular diffusion coefficients are several orders of magnitude larger in the gasphase ($\approx 10^{-5}$ m^2/s) than in the water phase ($\approx 10^{-9}$ m^2/s). The computation of the diffusivities for water vapor and the vapor of the contaminant is done using the binary diffusivities D_g^{aw}, D_g^{cw}, and D_g^{ac} (Falta et al., 1992) [20]

$$D_g^w = \frac{1 - x_g^w}{\frac{x_g^a}{D_g^{aw}} + \frac{x_g^c}{D_g^{cw}}} \tag{10}$$

$$D_g^c = \frac{1 - x_g^c}{\frac{x_g^w}{D_g^{cw}} + \frac{x_g^a}{D_g^{ac}}} \tag{11}$$

Since the diffusive fluxes J_g^K of the components have to meet the constraint

$$J_g^a + J_g^w + J_g^c = 0\,, \tag{12}$$

the diffusivity for the component air is not needed. The diffusive mole flux of the components in the gas phase is obtained by

$$J_g^K = -\varrho_{mol,g}\, D_{pm}^K \,\mathbf{grad}\, x_g^K \,, \tag{13}$$

where

$$D_{pm}^K = \tau \phi S_g D_g^K \,. \tag{14}$$

τ represents the tortuosity of the porous medium.

2.7 Relative Permeability

Approaches for the determination of relative permeabilities as a function of saturations in a two-phase system are well known, e.g. from Brooks and Corey (1964) [12] or van Genuchten (1980) [44]. For a three phase system, Parker et al. (1987) [36] suggest an approach for the NAPL relative permeability that is based on the two-phase parametrizations of van Genuchten:

$$k_{rn} = \sqrt{\frac{S_n}{1 - S_{wr}}} \cdot \left\{ \left(1 - S_{we}^{\frac{n}{n-1}}\right)^{\frac{n-1}{n}} - \left(1 - S_{te}^{\frac{n}{n-1}}\right)^{\frac{n-1}{n}} \right\}^2 \tag{15}$$

with

$$S_{we} = \frac{S_w - S_{wr}}{1 - S_{wr}} \tag{16}$$

$$S_{te} = \frac{S_w + S_n - S_{wr}}{1 - S_{wr}} \tag{17}$$

Eq. (15) does not explicitly consider the residual saturation S_{nr} of the NAPL phase. A modification of Eq. (15) can be achieved by replacing the tortuosity factor $\sqrt{\frac{S_n}{1-S_{wr}}}$ by $\sqrt{\frac{S_n - S_{nr}}{1-S_{wr}}}$. The water and gas phase relative permeabilities are calculated using the known two-phase relationships, since they are only dependent on their own saturations. Thereby, it is assumed that water is the wetting fluid with respect to NAPL and NAPL is wetting with respect to gas. Effects of hysteresis due to their enormous complexity are currently not considered in the model concept neither for relative permeability nor for capillary pressure, although in some cases they may have significant influence.

2.8 Capillary Pressure

Capillary Pressure in a three phase system is difficult to determine. Parker and Lenhard (1987) [35] give a capillary pressure model for a water–NAPL–gas system. Presuming that interfaces exist only between the phases water and NAPL respectively between NAPL and gas (according to their order of wettability), one can calculate the capillary pressures using the two-phase

approximations scaled by factors that consider the ratios of the surface tensions. The capillary pressure between NAPL and the water phase ($p_{c_{nw}}$) is thereby a function of S_w, whereas $p_{c_{gn}}$ is a function of $S_t = S_w + S_n$.

$$p_{c_{nw}}(S_w) = \frac{1}{\beta_{nw}} p_{c_{gw}} \tag{18}$$

and

$$p_{c_{gn}}(S_t) = \frac{1}{\beta_{gn}} p_{c_{gw}} \,. \tag{19}$$

The scaling factors β_{nw} and β_{gn} according to Lenhard (1994) [30] are calculated as:

$$\beta_{nw} = \frac{\sigma_{gn} + \sigma_{nw}}{\sigma_{nw}} \tag{20}$$

$$\beta_{gn} = \frac{\sigma_{gn} + \sigma_{nw}}{\sigma_{gn}} \tag{21}$$

In Eq. (20) and (21) σ represents the surface tension.

Then, from the total system pressure, which is equal to the pressure of the gas phase (p_g), the pressures of the NAPL and water phases can be obtained from:

$$p_n = p_g - \Theta p_{c_{gn}}(S_t) - (1 - \Theta) \left[p_{c_{gw}}(S_w) - p_{c_{nw}}(S_w = 1) \right] \tag{22}$$

$$p_w = p_n - \Theta p_{c_{nw}}(S_w) - (1 - \Theta) \left[p_{c_{nw}}(S_w = 1) \right] \tag{23}$$

$\Theta = min(1, \frac{S_n}{S_{nr}})$ ensures a continous transition from the three phase to the two phase system in case of disappearance of the NAPL phase.

This three phase capillary pressure approach of Parker and Lenhard (1987) [35] is based on the two phase relations of van Genuchten (1980) [44]. The influence of temperature on capillary pressure in porous media is not yet quantified sufficiently to implement relations therefore into our numerical model. Some rather qualitative suggestions therefore are found in Leverett (1941) [31] and in She and Sleep (1998) [41].

3 Basic Equations and Primary Variables

The mathematical description of the physical processes yields a system of coupled partial differential equations that exhibits a high degree of nonlinearity. Using an Eulerian approach we formulate for each of the mass components a single balance equation. In addition, presuming local thermal equilibrium, a single energy balance equation for the fluid-filled porous medium is required. The balance equations can be derived from the continuity condition where an enhanced Darcy Law for the determination of the fluid flow velocities is inserted (e.g., Helmig,

Table 1: Functional dependence of secondary variables on the primary variables

variables and functional dependence			
parameter	**phase**		
	gas	water	NAPL
mole fractions	$x_g^K(p_g, T)$	$x_w^K(p_g, T)$	assumption: $x_n^c = 1$
density	$\varrho_g(p_g, x_g^K, T)$	$\varrho_w(p_w, T)$	$\varrho_n(T)$
viscosity	$\mu_g(x_g^K, T)$	$\mu_w(T)$	$\mu_n(T)$
specific internal energy	$u_g(p_g, x_g^K, T)$	$u_w(p_w, T)$	$u_n(T)$
specific enthalpy	$h_g(p_g, x_g^K, T)$	$h_w(p_w, T)$	$h_n(T)$
molecular diffusion coefficient			
of water	$D_{pm}^w(p_g, S_g, T, \phi)$	-	-
of NAPL	$D_{pm}^c(p_g, S_g, T, \phi)$	-	-
relative permeability	$k_{rg}(S_g)$	$k_{rw}(S_w)$	$k_{rn}(S_g, S_w)$
capillary pressure	$p_{c_{gw}}(S_w, T)$	$p_{c_{gn}}(S_w, S_g, T)$	$p_{c_{nw}}(S_w, T)$
heat conductivity	$\lambda_{pm}(S_g, S_w, T)$		

parameters independent of primary variables
permeability K; porosity ϕ; specific heat capacity c_s and density ϱ_s of solid phase

1997 [25]). The equations are given in the following:

Mass:

$$\begin{aligned}
&\phi \frac{\partial (\sum_\alpha \varrho_{mol,\alpha} x_\alpha^K S_\alpha)}{\partial t} \\
&- \sum_\alpha \text{div} \left\{ \frac{k_{r\alpha}}{\mu_\alpha} \varrho_{mol,\alpha} x_\alpha^K \mathbf{K} (\mathbf{grad}\, p_\alpha - \varrho_{mass,\alpha} \mathbf{g}) \right\} \\
&- \text{div} \left\{ D_{pm}^K \varrho_{mol,g} \mathbf{grad}\, x_g^K \right\} \\
&- q^K = 0 \qquad K \in \{w, a, c\},\ \alpha \in \{w, n, g\}
\end{aligned} \tag{24}$$

Thermal Energy:

$$\begin{aligned}
&\phi \frac{\partial \left(\sum_\alpha \varrho_{mass,\alpha} u_\alpha S_\alpha\right)}{\partial t} + (1 - \phi) \frac{\partial \varrho_s c_s T}{\partial t} \\
&- \text{div}\ (\lambda_{pm}\, \mathbf{grad}\, T) \\
&- \sum_\alpha \text{div} \left\{ \frac{k_{r\alpha}}{\mu_\alpha} \varrho_{mass,\alpha} h_\alpha \mathbf{K} \left(\mathbf{grad}\, p_\alpha - \varrho_{mass,\alpha} \mathbf{g} \right) \right\}
\end{aligned}$$

$$-\sum_K \text{div}\left\{D_{pm}^K \varrho_{mol,g} h_g^K M^K \,\mathbf{grad}\, x_g^K\right\}$$

$$-q^h \;=\; 0 \qquad K \in \{w,a,c\},\ \alpha \in \{w,n,g\} \tag{25}$$

c_s represents here the specific heat capacity of the soil grains. The system of equations is completed by the supplementary constraints given already in Section 2.

The number of degrees of freedom in a multiphase multicomponent system is, according to the Gibbsian phase rule

$$F = K - P + 2 + (P-1) = K + 1 \tag{26}$$

with K and P representing the number of phases and components. In our case, this requires the choice of four independent primary variables to determine the thermodynamic state of the system. For all possible phase states, pressure and temperature can be used as primary variables. In case of all three fluid phases being present, the saturations of water and NAPL complete the set for this phase state. If a phase disappears, one of the primary variables 'saturation' is replaced by a 'mole fraction' (Tab. 2). An example for this is shown in Fig. 3. At time t_0, all nodes of the element have phase state 1 (all three fluid phases present). Assuming a steam front propagating in x–direction, one can see that the front has not yet reached the element. At time $t_0 + \Delta t$, the temperature at one of the nodes has reached the boiling temperature of pure water, and the NAPL saturation has become zero, which means that the NAPL phase has disappeared at this node.

In order to describe the disappearance and appearance of phases, we need a process adaptive algorithm for the substitution of the primary variables. Its implementation in MUFTE_UG is given schematically in Fig. 4.

Checking the phase states requires the definition of criteria for the indication of changes. The simplest of all cases is given when one of the phases disappears. Then its saturation takes a negative value. It's more complex for the appearance of a fluid phase. Different cases have to be distinguished (Tab. 2).

If the gas phase is present (phase states 1, 3, 5, 6), then water respectively NAPL can appear as liquid, when the partial pressure of their corresponding vapor in the gas phase exceeds the respective saturation pressure. If only the water phase is present (2), the appearance of NAPL can be noticed, when the mole fraction of the NAPL in water exceeds the solubility χ_w^c. An appearance of the gas phase occurs, when the sum of the (hypothetical) vapor pressures of the individual components becomes higher than the total pressure, which is given by p_g (hypothetical gas phase pressure). The contribution of the air component can be obtained by transforming Eq. (5) as 'Henry coefficient' times 'mole fraction of air in water'. E.g., degasing of carbon dioxide (CO_2) due to pressure lowering can also be modeled in such manner.

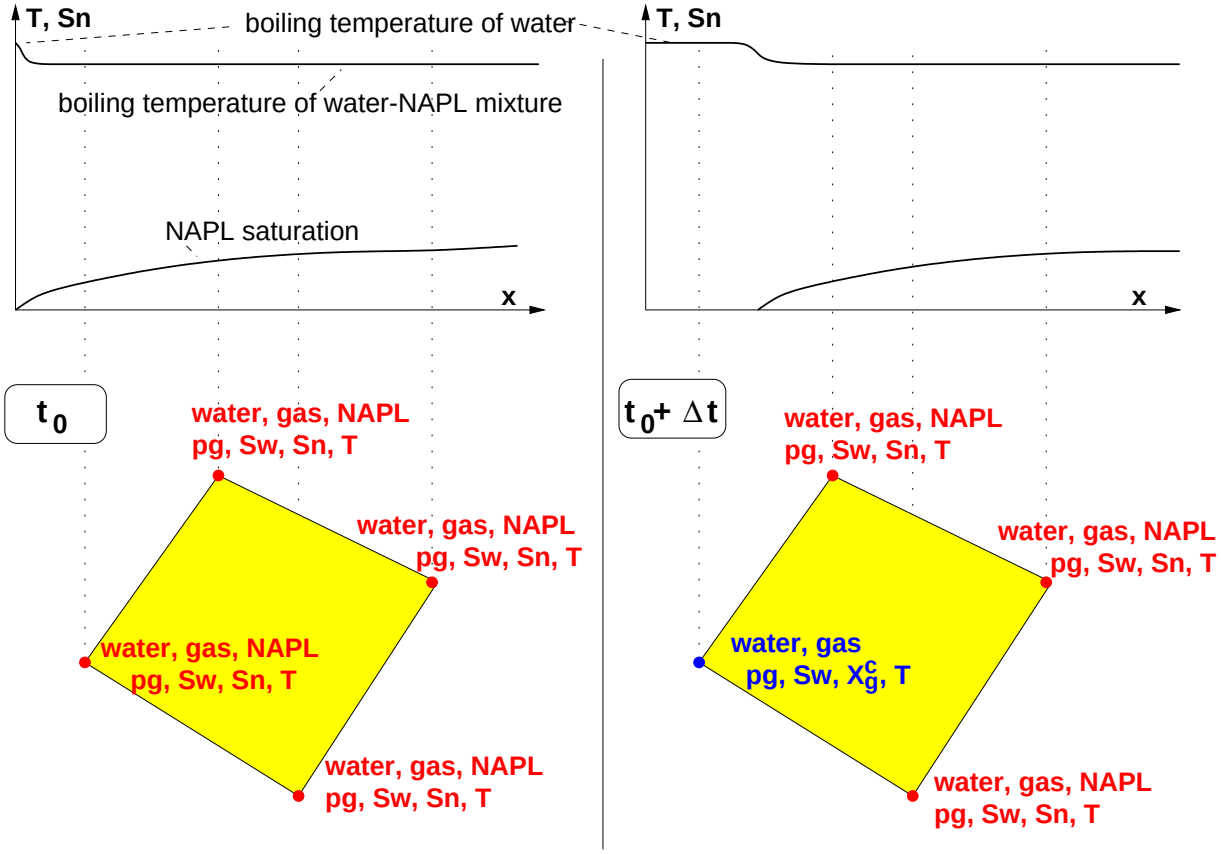

Figure 3: Process adaptive substitution of primary variables after a change of phase state

The saturation pressure criterion for indicating the appearance of the water or NAPL phase shows satisfactory performance for condensation dominated processes (Class, 2000 [15]). Our experiences with advection dominated processes exhibited some numerical problems leading to small time steps. There is still need for analyzing the responsible physical processes and their

Table 2: Phase states, corresponding primary variables, and criteria for the substitution in case of phase appearance

phase state	present phases	primary variables	appearance of phase		
			water	NAPL	Gas
1	w, n, g	S_w, S_n, p_g, T	-	-	-
2	w	x_w^c, x_w^a, p_g, T	-	$x_w^c > \chi_w^c$	$p_{sat}^w + H_w^a x_w^a > p_g$
3	n, g	S_n, x_g^w, p_g, T	$x_g^w p_g > p_{sat}^w$	-	-
4	w, n	S_n, x_w^a, p_g, T	-	-	$p_{sat}^w + p_{sat}^c + H_w^a x_w^a > p_g$
5	g	x_g^c, x_g^w, p_g, T	$x_g^w p_g > p_{sat}^w$	$x_g^c p_g > p_{sat}^c$	-
6	w, g	x_g^c, S_w, p_g, T	-	$x_g^c p_g > p_{sat}^c$	-

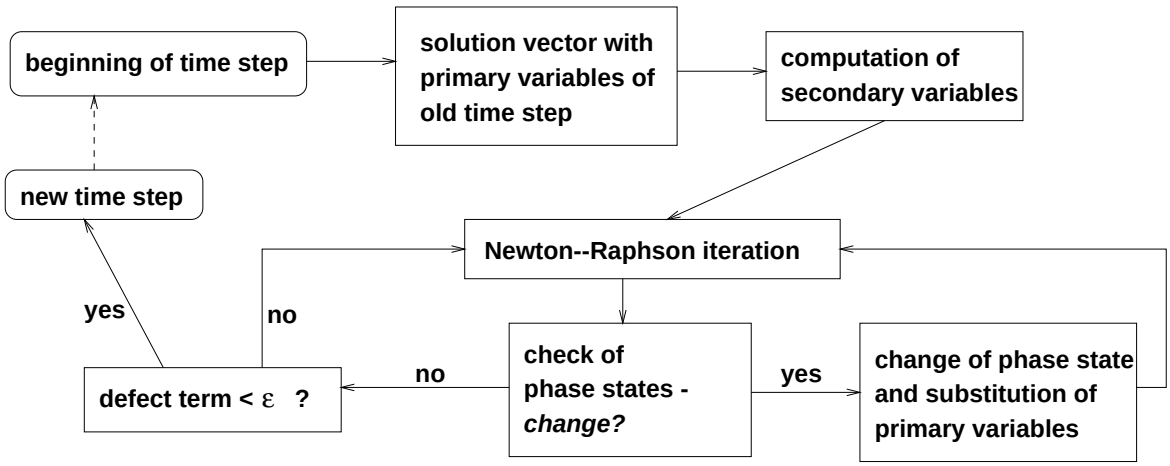

Figure 4: Algorithm for the substitution of the primary variables during the computation of a time step

mathematical/numerical implementation.

For time discretization we use a fully implicit Euler method. For the spatial discretization of Eq. (24) und (25) we implemented two different mass conservative schemes, namely a Control-Volume-Finite-Element method (CVFE) and a Subdomain Collocation Method (BOX) (e.g., Helmig, 1997 [25]; Class, 2000 [15]). Both methods can be derived from the principle of weighted residuals. The difference between CVFE and BOX results from the choice of the weighting functions. For CVFE the weighting functions are equal to the shape functions, whereas for BOX a piecewise constant weighting of the residuals is done. Both methods use a mass lumping which avoids the occurence of non-physical oscillations of the solution (Celia and Binning, 1992 [13]). A fully-upwind weighting of the advective flux term coefficients is also applied for both schemes. CVFE and BOX yield different results when the main flow direction deviates from the orientation of the elements. Say a given model domain is discretized with regular rectangular elements. The main flow direction be along the diagonals of the rectangles. Then the BOX method, which represents a 5-point stencil, can not reproduce fluxes between the end points of the element diagonal. Instead, one gets numerical cross diffusion into the system. CVFE is able to model these diagonal fluxes directly, however for coarse grids an increased rate of numerical dispersion in this direction is obtained. Due to the diffusive behaviour of heat conduction the distribution of temperature is less influenced by the choice of the discretization method than the distribution of saturations. Thus, temperature is in this context a rather good natured quantity.

The nonlinearities in the equations are handled with a Newton–Raphson method, where the elements of the Jacobian matrix are computed by numerical differentiation (see also Section 4).

4 Extension of the Multigrid Method

For the solution of the linearized system of equations, which may have a huge number of unknowns, fast and efficient solution techniques are required to reduce computation time. Multigrid methods (e.g., Hackbusch, 1985 [23]) are very fast methods for solving large sparse systems of linear equations arising from discretized partial differential equations. Their order of convergence is, when applied to elliptic model problems, independent of the mesh size, i.e., solving a system of linear equations requires computer time, which is proportional to the number of unknowns. The work of Bastian and Helmig (1999) [7] shows a very satisfactory performance for a multigrid method applied to the linearized fully coupled two-phase flow equations, although a convergence proof for such systems is not available. The extension of the multigrid method for multiphase multicomponent systems with variable phase states requires a reformulation of the prolongation algorithms taking into consideration that the set of primary variables at the nodes inside an element may not be consistant.

4.1 Basic algorithms

For a more detailed explanation of the discretization and solution methods implemented in MUFTE_UG we recommend, e.g., Bastian (1999) [5] or Bastian and Helmig (1999) [7].
A damped inexact Newton algorithm for solving the nonlinear system of equations is given by:

Choose $x^{k+1,0}$; set $m = 0$;
while $(||F(x^{k+1,m})||_2 \;/\; ||F(x^{k+1,0}||_2 > \varepsilon_{nl}))$
{
  Solve $K(x^{k+1,m})u = -F(x^{k+1,m})$
    with accuracy ε_{lin};
  $x^{k+1,m+1} = x^{k+1,m} + \eta u$;
  $m = m + 1$;
}

$F(x^{k+1,m})$ represents the defect term obtained at time level $k+1$ and iteration m depending on the nonlinear functions F and the vector of primary variables x. ε_{nl} and ε_{lin} are the accuracy criteria of the nonlinear respectively the linear solution. $||\cdot||$ is the Euclidean vector norm. The damping factor $\eta = (1/2)^q$ is chosen such that

$$||F(x^{k+1,m+1}||_2 \leq \left[1 - \frac{1}{4}\left(\frac{1}{2}\right)^q\right] ||F(x^{k+1,m}||_2 \tag{27}$$

is valid for the smallest possible $q \in \{0, 1, ..., n_{ls}\}$ with the maximum number of line search steps n_{ls} being between 4 and 6. A time step reduction is applied if no such q can be found.

$$Ku = f \tag{28}$$

is the Jacobian system to be solved by a linear solver. The multigrid mesh hierarchy yields a Jacobian system on each grid level l. We need linear mappings, restriction R_l and prolongation P_l, for interpolation between the grid levels. A multigrid algorithm (V-cycle) for an iterative improvement of a given vector u_l can be written as follows:

mgc (l, u_l, f_l)
{
  if $(l == 0)$ $u_0 = K_0^{-1} f_0$;
  else {
    Apply ν_1 smoothing iterations to $K_l u_l = f_l$;
    $d_{l-1} = R_l(f_l - K_l u_l)$;
    $e_{l-1} = 0$;
    mgc $(l-1, e_{l-1}, d_{l-1})$;
    $u_l = u_l + P_l e_{l-1}$;
    Apply ν_2 smoothing iterations to $K_l u_l = f_l$;
  }
}

For smoothing iterations, e.g., $\nu_1 = \nu_2 = 2$ ILU steps (incomplete decomposition, e.g., *Hackbusch*, 1985) can be chosen.

4.2 Prolongation adaptive to the phase states

Let e_{l-1}^m be the error, i.e., the deviation of u_{l-1}^m from the exact solution, on level $l-1$. Then, the coarse grid correction can be written as an iteration of form:

$$u_l^{m+1} = u_l^m + I_{l-1}^l e_{l-1}^m \ , \tag{29}$$

where matrix I_{l-1}^l describes the transfer (prolongation) between levels $l-1$ and l. For the prolongation of the coarse grid corrections, one has to take into account that different phase states are inherent with different primary variables in the solution vectors. Thus, it may occur that the correction for a fine grid node has to be interpolated from coarse grid nodes with different phase states. Fig. 5 illustrates this case.

It shows a NAPL-contaminated subdomain, which is recoverd by a steam/air injection. The subdomain is discretized with a coarse grid element (1-2-3-4) respectively four fine grid elements (I-II-III-IV; II-V-VI-III and so on). The NAPL-contaminated area represents a three-phase area and has phase state 1 (NWG). The area already cleaned up only contains the phases water and gas and has therefore phase state 6 (WG). Thus, the coarse grid nodes 1, 2, and 4 have phase

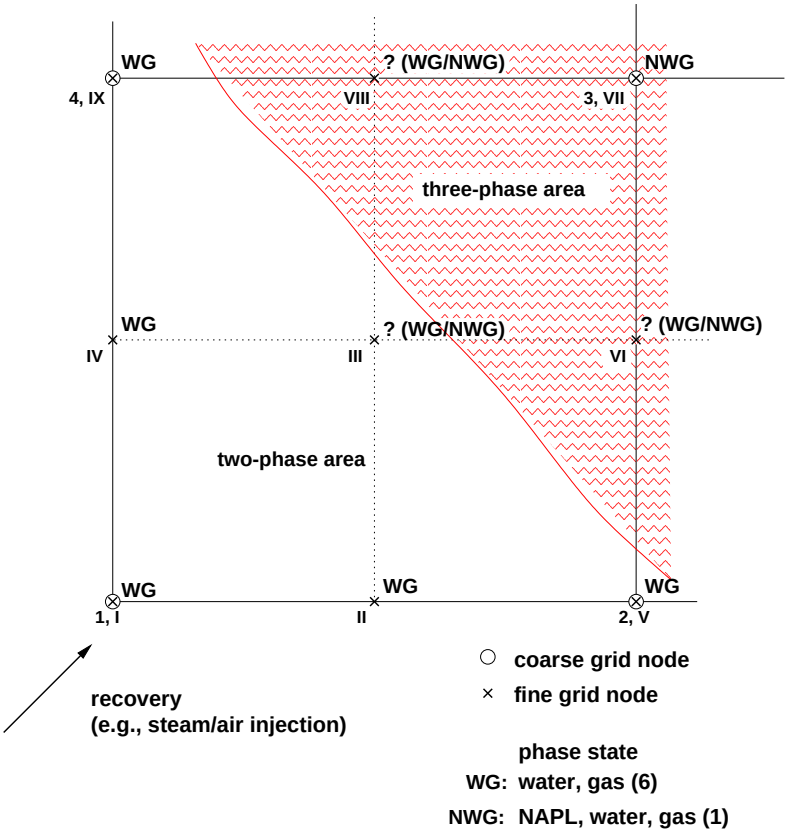

Figure 5: Prolongation dependent on the phase states

state WG, whereas node 3 still has NWG. We assume that the fine grid node III has phase state WG. Then, the correction of the primary variables (p_g, S_w, x_g^c, T) can be interpolated directly from the coarse grid nodes 1, 2, and 4. However, the vector of primary variables at node 3 contains x_g^c instead of S_n (phase state NWG). Thus, the correction value of coarse grid node 3 for the primary variable S_n has to be transformed into a correction value for the primary variable x_g^c at fine grid node III. This can be achieved by a linearization of the correction around the corresponding position in the solution vector in iteration m:

$$e^m|_{x_j} = f_{x_j}(u^i + e^i) - f_{x_j}(u^i) \tag{30}$$

$e^m|_{x_j}$ is the correction of variable x_j. f_{x_j} stands for the function through which x_j can be computed from the given primary variables. In case of node III, $e^m|_{x_j}$ equals the correction value of variable x_g^c from the interpolation part of node 3. $e^m|_{x_g^c}$ at node 3 is computed using the functional $f_{x_g^c} = p_{sat}^c / p_g$.

The existence of a hierarchical grid system can be used for another efficient solution method. Applying *nested iterations* provides the possibility to use approximate values for u_{l-1} from an iteration on grid level $l-1$ as starting values u_l for the iteration on grid level l. Thus, by improving the starting values one obtains better results of the iteration reducing the iteration

steps necessary for a given accuracy. For large systems this thereby improved convergence behaviour outweighs the apparently higher computation effort rapidly. Since a phase state must be assigned to every node, we need rules to determine the phase states of fine grid nodes, which are not part of the coarser grid. A look on Fig. 5 shows that fine grid nodes I, V, VII, IX are identical with coarse grid nodes 1, 2, 3, 4 and therefore inherit the respective phase states. For fine grid nodes II, III, IV, VI, VIII, the phase states must be determined from the current state of the system. In a first approach, we evaluate the Ansatzfunctions of the coarse grid elements with respect to a given fine grid node and take the phase state from the coarse grid node with the highest Ansatzfunction value. This leaves still doubt wether the achieved choice of the respective coarse grid node is unique (e.g., nodes III and VI in Fig. 5). Our next step in this context is developing better criteria for assigning the phase states to fine grid nodes, e.g., by evaluating the phase velocities and transport rates around a node of interest.

5 Examples

5.1 Verification: The Heatpipe Effect

For our model concept for nonisothermal water–NAPL–gas flow in a porous medium, there exist no analytical solutions that would allow a comprehensive verification. Instead, one has to split the task of verification into parts which allow verification by means of analytical solutions of subproblems and parts which use well-controlled experiments for comparison with numerical results. The latter is commonly referred to as validation and will be discussed in PAPER II.

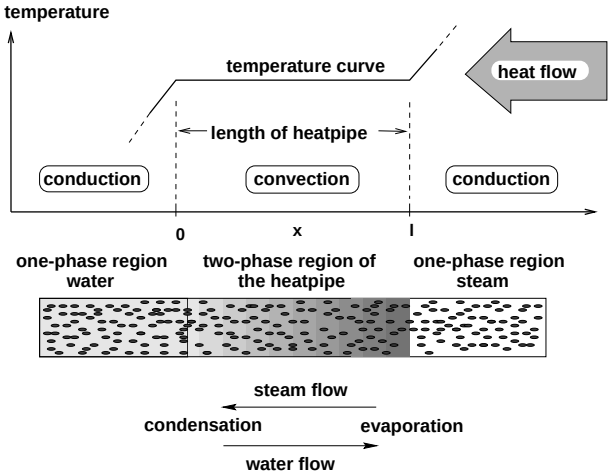

Figure 6: The heatpipe effect: schematic description

Udell and Fitch (1985) [42] provide a semi-analytical solution for a nonisothermal water–gas system in a porous medium, in which the heat transfer processes convection, conduction, and

diffusion as well as capillary forces play an essential role. This semi-analytical solution is practical for comparison with numerical results (Emmert, 1997 [18]). At the right-hand boundary of a horizontal column (Fig. 6) with an initially constant water saturation of 0.5, a constant heat flux ($q = 100$W) into the column is given. At the left-hand boundary constant values (Dirichlet conditions) for the gas phase pressure ($p_g = 101330$Pa), the effective water saturation ($S_{we} = 1.0$), and the air mole fraction in the gas phase ($x_g^a = 0.71$). Thus, the temperature is also stated to $T = 68.6°$C. Due to the heat flux the system is heated up until the boiling temperature is reached and steam is built at the right-hand boundary. This causes a pressure gradient in the gas phase and the steam flows away from the heat source. After reaching cooler regions of the column, the steam condenses and sets free its latent heat of vaporization. After a while, a non-uniform saturation profile is obtained and a gradient of the capillary pressure is produced. Hence, the pressure gradients of the phases have opposite directions and a circulation flow is built. After reaching a stationary system state, three regions can be distinguished, each of them associated with a dominant heat transport process (Fig. 6). Udell and Fitch (1985) [42] derive four coupled first order differential equations for pressure, saturation, temperature and gas-phase mole fraction. These equations are solved by numerical integration with a fourth order Runge–Kutta method.

The numerical simulation of the heatpipe system was carried out with the BOX discretization method. Note, that the choice, wether BOX or CVFE is used, makes no difference for the present one-dimensional case. The following model parameters were used for the simulation run:

Permeability	: $K = 10^{-12}$ m^2
Porosity	: $\phi = 0.4$
Residual water saturation	: $S_{wr} = 0.15$
heat conductivity of the fully-saturated porous medium	: $\lambda_{pm}^{S_w=1} = 1.13$ W/(m K) (see Eq. 9)
heat conductivity of the dry porous medium	: $\lambda_{pm}^{S_w=0} = 0.582$ W/(m K) (see Eq. 9)
Soil grain density	: $\varrho_s = 2600$ kg/m^3
Specific heat capacity of the soil grains	: $c_s = 700$ J/(kg K)
Density of water	: $\varrho_w = 958.4$ kg/m^3
Dynamic viscosity of water	: $\mu_w = 2.938 \cdot 10^{-4}$ Pa s
Dynamic viscosity of air	: $\mu_g^a = 2.08 \cdot 10^{-5}$ Pa s
Dynamic viscosity of steam	: $\mu_g^w = 1.20 \cdot 10^{-5}$ Pa s

A function according to Fatt and Klikoff (1959) [21] is chosen for the relative permeability–saturation relationship:

$$\begin{aligned} k_{rg} &= (1 - S_e)^3 \quad \text{for steam (gas phase)} \\ k_{rw} &= S_e^3 \quad \text{for water} \end{aligned} \tag{31}$$

For the capillary pressure–saturation relationship, the following function of Leverett (1941) [31] is used:

$$p_c = p_0 \cdot \gamma \cdot 1.417(1 - S_e) - 2.120(1 - S_e)^2 + 1.263(1 - S_e)^3 \tag{32}$$

The surface tension γ at $T = 100.5°\text{C}$ is 0.05878 Nm^{-1} and for the scaling pressure applies $p_0 = \sqrt{\phi/K}$. A constant value of 0.5 is assigned to the tortuosity τ and the binary diffusion constant D_g^{aw} takes the value $2.6 \cdot 10^{-6}$ m^2/s.
The dimension of the model domain in x–direction is chosen to 2.4 m. However, this is not important for the length of the heatpipe after reaching stationary state as long as the domain is sufficicently large for the heatpipe to be built. We used a discretization length of $\Delta x = 0.04$ m. The initial conditions were chosen to $p_g = 101330$ Pa, $S_w = 0.5$ und $T = 70°\text{C}$.

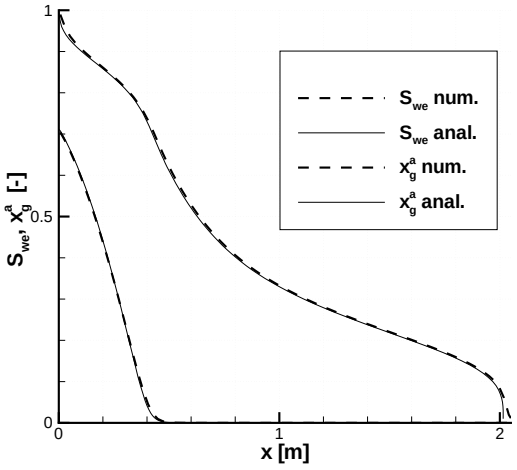

Figure 7: Semi-analytical and numerical curve of S_{we} and x_g^a

The results of the numerical simulation with the semi-analytical solution are compared in Fig. 7, 8, and 9. In all cases, the curves match very well. The length of the heatpipe is obtained to $\approx$ 2.0m consistently. Due to the complex interaction of different physical processes and the excellent agreement between simulation and semi-analytical solution, we state that the verification of the numerical model for an air–water system was successfull. Starting with the given initial conditions, the model could reproduce the heating at the right-hand boundary from 70°C up to the boiling temperature. Also the gradual extension of the heatpipe region until reaching the stationary system state was modeled correctly. The disappearance of the water phase associated with a change of the phase state and a substitution of the primary variables was carried out well. Fig. 9 shows clearly that the pressure gradients of both phases are oppositely directed.

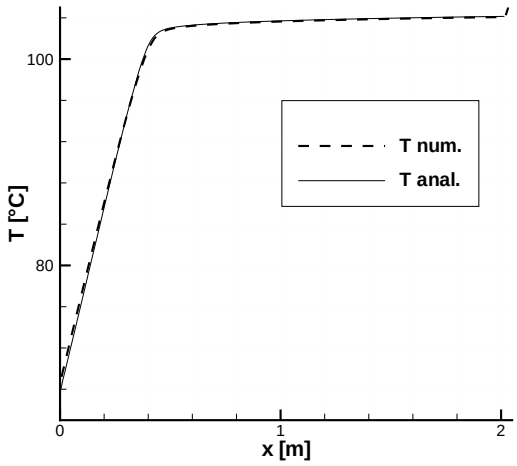

Figure 8: Semi-analytical and numerical curve of T

5.2 Performance of the Multigrid: The Fivespot Problem

In the following we present an example for the comparison of the multigrid method with a classical iteration method (ILU scheme) as preconditioners for a BiCGStab solver.

Fig. 10 shows a two-dimensional model domain (1 m $\times$ 1 m). The coarsest grid used in the multigrid hierarchy is given with 400 quadratic elements. Any refinement of an element yields four quadratic elements on the next finer grid level (regular refinement, e.g. *Bastian*, 1999). The system is initially contaminated with xylene in residual saturation. Furthermore, there is a water saturation slightly below residual saturation and atmospheric pressure at a temperature of 293.15 K. In the lower left corner a steam/air mixture is injected (Neumann boundary condition); in the upper right corner the system is open to the environment (Dirichlet boundary condition). The remaining boundary has no-flow properties.

The boundary conditions in the corners are each assigned constant to 0.05 m along the domain boundaries which corresponds to the node distance on the coarsest grid:

- lower left: Neumann boundary condition

$$q^w = -1.0 \text{ mol/(s m)}$$
$$q^a = -3.0 \text{ mol/(s m)}$$
$$q^h = -50000 \text{ J/(s m)}$$

- upper right: Dirichlet boundary condition

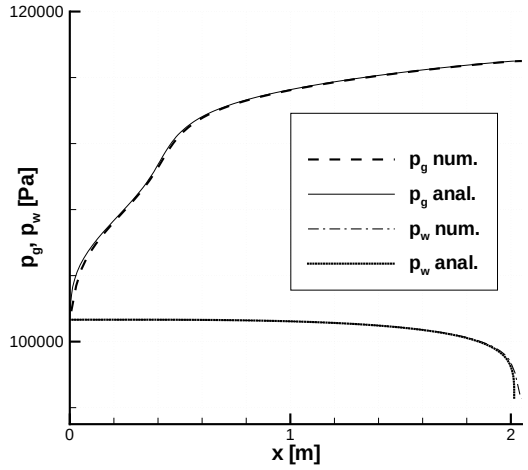

Figure 9: Semi-analytical and numerical curve of p_g and p_w

$S_n = 0.1$
$S_w = 0.1$
$p_g = 101300$ Pa
$T = 293.15$ K

The initial conditions are the same as the Dirichlet conditions given in the upper right corner (phase state 1: water, NAPL, and gas phases are present).

Further system parameters:

permeability	$K = 1.0 \cdot 10^{-10}$ m^2
porosity	$\phi = 0.45$
water residual saturation	$S_{wr} = 0.12$
NAPL residual saturation	$S_{nr} = 0.10$
gas residual saturation	$S_{gr} = 0.00$
heat conductivity	$\lambda_{pm}^{S_w=S_n=0} = 0.35$ J/(m s K)
	$\lambda_{pm}^{S_w=1} = 1.60$ J/(m s K)
	$\lambda_{pm}^{S_n=1} = 0.65$ J/(m s K)
density of soil grains	$\varrho_s = 2650$ kg/m^3
spec. heat capacity of soil grains	$c_s = 850$ J/(kg K)

Gravitation and capillary forces were neglected. For the relative permeability–saturation relationship we applied the approaches of *Parker et al* (1987) respectively *van Genuchten* (1985).

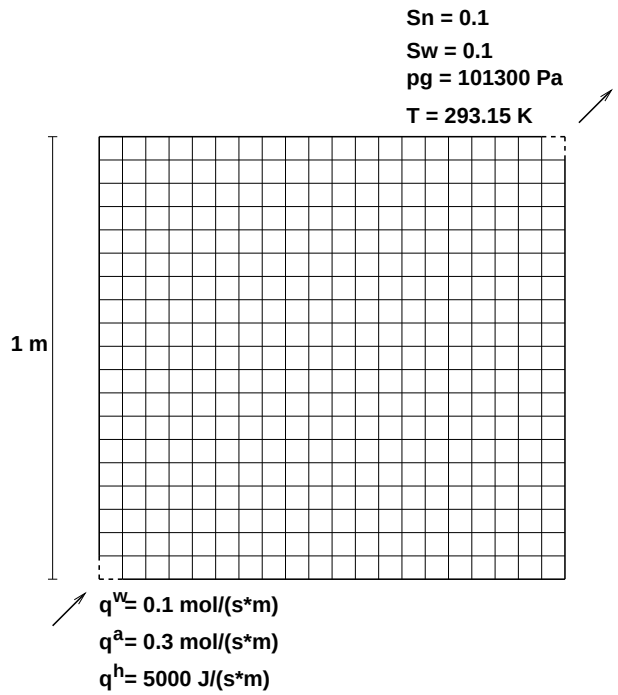

Figure 10: The fivespot problem (coarse grid: 400 elements)

The van Genuchten parameter n was assumed to be $n = 4.0$.

Fig. 11 shows the distribution of NAPL saturation and temperature after 3 hours of steam/air injection. One can see that the domain is cleaned up from the lower left corner. The evaporated NAPL is transported in the gas phase towards the upper right corner. When reaching the cooler regions part of the NAPL vapor condenses such that the liquid NAPL phase accumulates forming a peak of NAPL saturation. The temperature plot shows that in the subregion already cleaned up an almost constant temperature of $\approx$330 K prevails, which is equal to the temperature of the injected steam/air mixture. A change of the phase state from NWG (1) to WG (6) occurs whenever the NAPL saturation disappears at a node.

In the following case study we investigated wether the application of the extended multigrid method to this complex three-phase three-component system yields comparable solution performance as known from the literature (e.g., Hackbusch, 1985 [23]) for elliptic problems. The following four combinations of solvers for the linearized equations are compared:

1. Nested iteration, multigrid V-cycle preconditioner with $\nu_1 = \nu_2 = 2$ smoothing iterations (ILU), BiCGStab solver for finest grid, direct solver as coarse grid solver (for computation of the correction on the coarsest grid)

2. Same as Case 1, but nested iteration only for the computation of the first time step

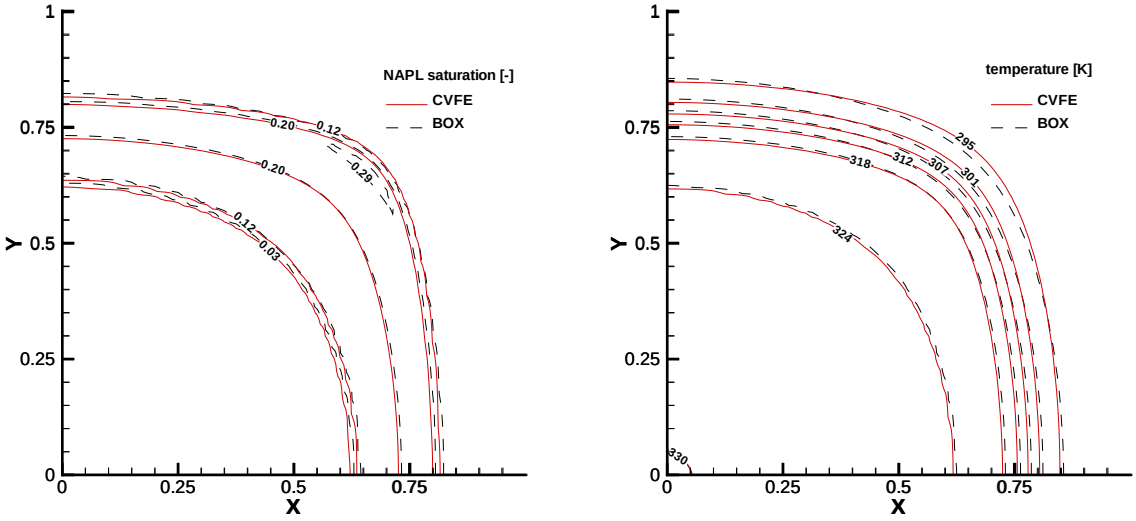

Figure 11: Isolines of NAPL saturation (left) and temperature (right) after 3 hours simulation time

3. ILU as preconditioner, BiCGStab solver for finest grid, nested iteration only for the computation of the first time step

4. direct solver for the finest grid, no nested iteration

We applied for the criteria of linear and nonlinear accuracy (ε_{lin} and ε_{nl}) a value of 10^{-4}. The simulations were conducted on different refinement levels. The coarsest grid contains 400 quadratic elements, the refinement levels 1, 2, 3, and 4 accordingly have 1600, 6400, 25600, and 102400 elements. Each of the simulations ended at simulation time 14400 s (4 hours). The application of the direct solver exhibits already at refinement level 1 (1600 elements) an increase in computation time compared to all other cases by a factor of 5. In Tab. 3, 4, and 5 some characteristic performance statistics are listed for Cases 1, 2, and 3. The abbreviations used are explained shortly:

SIZE	number of elements on the finest grid
avg. Δt	average time step size [s]
EXECT	execution time [s]
NLIT	number of required nonlinear iteration steps
LIT	number of required linear iteration steps
AVG	= LIT/NLIT: average number of linear iteration steps per nonlinear iteration step
MAXLIT	maximum number of linear iteration steps during a nonlinear iteration step

Table 3: Simulation parameter Case 1

SIZE	avg. Δt	EXECT	NLIT	LIT	AVG	MAXLIT
1600	350	7561	317	582	1.84	4
6400	306.3	$3.48 \cdot 10^4$	615	1435	2.33	5
25600	248.9	$1.95 \cdot 10^5$	1172	3083	2.63	5
102400	181.2	$1.27 \cdot 10^6$	2277	6368	2.80	5

Table 4: Simulation parameter Case 2

SIZE	avg. Δt	EXECT	NLIT	LIT	AVG	MAXLIT
1600	254.8	8126	252	765	3.04	5
6400	121.3	$6.28 \cdot 10^4$	526	2072	3.94	6
25600	54.7	$5.16 \cdot 10^5$	1160	4781	4.12	6
102400	19.5	$5.25 \cdot 10^6$	3056	12265	4.01	7

Discussion of the results: The average time step size in Case 1 (nested iteration for all time steps) with increasing refinement level becomes significantly larger than for the other cases. The maximum time step length was chosen to $\Delta t_{max} = 350$ s. There is an automatic time step control implemented in MUFTE_UG, which halfens the time step if no convergence within the nonlinear Newton solver is achieved. Normally, a reduction of the space discretization length is accompanied with a reduced time step length. The use of nested iterations enables an improved starting value for the iteration such that a better convergence behavior is obtained permitting larger time step sizes. The dependence of the computing effort on the refinement level is almost reached by the multigrid method in the manner as it would be expected for elliptic problems. Convergence should be achieved independently of the refinement level. Thus, the computing effort should increase proportionally to the number of nodes (number of unknowns), i.e., the value of AVG should be asymptotically constant. However, the ratio of linear to nonlinear iteration steps (AVG) is clearly better in Case 1 than in Case 2. The reason therefore is probably that the starting values for the iteration are given better when using nested iteration. With increasing SIZE this effect of better linear convergence has an important influence on the total execution

Table 5: Simulation parameter Case 3

SIZE	avg. Δt	EXECT	NLIT	LIT	AVG	MAXLIT
1600	254.8	8288	252	12307	48.84	70
6400	121.3	$9.42 \cdot 10^4$	526	50505	96.02	141
25600	54.7	$1.18 \cdot 10^6$	1160	207033	178.48	318

time (EXECT). For 1600 elements the computation time has the same order of magnitude for all three cases ($\approx$ 8000 s). The more grid levels are used, the more computation time can be saved compared to the ILU scheme when using the multigrid preconditioner or even nested iteration. The ILU/BiCGStab scheme (Case 3) confirms the expected convergence behavior ($\rho = 1 - \mathcal{O}(h)$). The number of maximum linear iteration steps (MAXLIT) during a single Newton step roughly doubles with each refinement level, whereas it remains nearly constant for Cases 1 and 2. The computation effort for one multigrid step is approximately by a factor of 4 larger than for one ILU/BiCGStab step. But this is only a disadvantage for small refinement levels. Since the convergence behavior of the multigrid method was nearly textbooklike, it could outweigh this for higher levels of refinement and yield significant savings in computation time.

6 Conclusions and Outlook

In this paper, a three-phase three-component model concept for the simulation of nonisothermal water-gas-NAPL systems is presented. Variable phase states are considered using an algorithm for the process adaptive switching of the primary variables according to the phase states. A verification example is given for an air-water system (heatpipe effect). A multigrid method was extended in order to apply to this specific problem and a comparison with an ILU scheme was conducted with respect to solution performance.

The verification can be carried out only for sub-problems of the present model concept. In particular, the interaction between all three phases and temperature effects is not described by analytical or semi-analytical solutions in the literature. It is therefore important to use well-controled experiments in order to validate the model as possible. We refer here to PAPER II, where model validation and the applicability of the model for practical problems are discussed.

The example given in the previous section showed that a successful application of multigrid methods is possible also for the multiphase multicomponent model concept with variable phase states. A further improvement of the convergence is expected when the prolongation of the phase states is done depending on the flow directions and velocities of the phases. An important basic step could be made in order to provide fast and efficient solution methods for these complex physical systems and the mathematical equations arising from this. For practical application of such complex models to field scale problems, this is an essential precondition, since the number of unknowns may reach huge numbers very fast. The program system MUFTE_UG provides further the possibility of a parallelization (e.g. Bastian, 1996 [4]; Birken and Bastian, 1994 [11]). In future work we want to improve the robustness of the substitution algorithm for the primary variables. Experience with the developed code showed that problems may arise in the case of appearing phases due to displacement processes. An intensive analysis of the physical processes together with the mathematical description will be necessary therefore.

The model concept described in this paper builds the basis for further currently ongoing research work, e.g., dealing with degassing processes in the near-field of nuclear waste disposal sites (Bastian et al., 2000 [6]) or degassing of methane in submarine aquifers (Sheta et al, 2001).

References

[1] A.E. Adenakan, T.W. Patzek, and K. Pruess. Modeling of Multiphase Transport of Multicomponent Organic Contaminants and Heat in the Subsurface: Numerical Model Formulation. *Water Resour. Res.*, 29:3727–3740, 1993.

[2] K. Aziz, A.B. Ramesh, and P.T. Woo. Fourth SPE Comparative Solution Project: Comparison of steam injection simulators. *Journal of Petroleum Technology*, 1987.

[3] K. Aziz and A. Settari. *Petroleum Reservoir Simulation.* Applied Science Publishers, London, 1979.

[4] P. Bastian. *Parallele Adaptive Mehrgitterverfahren.* Teubner Verlag, Stuttgart, 1996.

[5] P. Bastian. Numerical Computation of Multiphase Flows in Porous Media. Habilitationsschrift vorgelegt an der Technischen Fakult"at der Christian–Albrechts–Universit"at Kiel, 1999.

[6] P. Bastian, Z. Chen, R.E. Ewing, R. Helmig, H. Jakobs, and V. Reichenberger. Numerical simulation of multiphase flow in fractured porous media. In *Lecture Notes in Physics*, pages 80–92. Springer Verlag, 2000.

[7] P. Bastian and R. Helmig. Efficient Fully-Coupled Solution Techniques for Two Phase Flow in Porous Media. Parallel Multigrid Solution and Large Scale Computations. *Adv. Water Resour.*, 23:199–216, 1999.

[8] J. Bear. *Dynamics of Fluids in Porous Media.* Elsevier, New York, 1972.

[9] C. Betz, A. Färber, C.M. Greene, H.-P. Koschitzky, and R. Schmidt. Removing volatile and semivolatile contaminants from the unsaturated zone by injection of a steam/air-mixture. In *Proceedings of the 6th International SZK/TNO Conference "Contaminated Soil'98"*, pages 575–584, Edinburgh, UK, 1998.

[10] A. Bielinski. Numerische Modellierung von Strömungs- und Transportvorgängen für Mehrphasen/Mehrkomponenten–Systeme in geklüftet–porösen Medien. Master's thesis, Institut für Wasserbau, Universität Stuttgart, 2001.

[11] K. Birken and P. Bastian. *Dynamic Distributed Data - Spezifikation und Funktionalit"at.* RUS, Universit"at Stuttgart, 1994.

[12] A.N. Brooks and A.T. Corey. Hydraulic Properties of Porous Media. In *Hydrol. Pap.* Fort Collins, Colorado State University, 1964.

[13] M.A. Celia and P. Binning. A Mass Conservative Numerical Solution for Two–Phase Flow in Porous Media With Application to Unsaturated Flow. *Water Resour. Res.*, 28:2819–2828, 1992.

[14] H. Class. Numerical Simulation of Non-Isothermal Steam Injection Processes in NAPL-Contaminated Porous Media. In *Proceedings of the 28th IAHR Congress*, Graz, 1999.

[15] H. Class. *Theorie und numerische Modellierung nichtisothermer Mehrphasenprozesse in NAPL–kontaminierten porösen Medien.* PhD thesis, Institut für ComputerAnwendungen im Bauingenieurwesen, Technische Universität Braunschweig, 2000.

[16] K.H. Coats. Simulation of steamflooding with distillation and solution gas. *Society of Petroleum Engineers Journal*, October 1976.

[17] K.H. Coats, W.D.G. Chieh Chu, and B.E. Marcum. Three–dimensional simulation of steamflooding. *Society of Petroleum Engineers Journal*, December 1974.

[18] M. Emmert. *Numerische Simulation von isothermen/ nichtisothermen Mehrphasenprozessen unter Berücksichtigung der Veränderung der Fluideigenschaften.* PhD thesis, Institut für Wasserbau, Universität Stuttgart, 1997.

[19] R.W. Falta, K. Pruess, S. Finsterle, and A. Battistelli. T2VOC User's Guide. Technical report, Lawrence Berkeley National Laboratory, 1995. LBL-36400.

[20] R.W. Falta, K. Pruess, I. Javandel, and P.A. Witherspoon. Numerical Modeling of Steam Injection for the Removal of Nonaqueous Phase Liquids From the Subsurface. 1. Numerical Formulation. *Water Resour. Res.*, 28,2:433–449, 1992.

[21] I. Fatt and W.A. Klikoff. Effect of fractional wettability on multiphase flow through porous media. *AIME Transactions*, 216:246, 1959.

[22] P.A. Forsyth. Three dimensional modeling of steam flush for DNAPL site remediation. Technical report, Dep. of Computer Science, University of Waterloo, 1993. CS-93-56.

[23] W. Hackbusch. *Multi–grid methods and applications.* Springer Verlag, Berlin, 1985.

[24] R. Helmig. *Theorie und Numerik der Mehrphasenströmungen in geklüftet–porösen Medien.* PhD thesis, Institut für Strömungsmechanik und Elektronisches Rechnen im Bauwesen, Universität Hannover, Bericht Nr. 34, 1993.

[25] R. Helmig. *Multiphase Flow and Transport Processes in the Subsurface - A Contribution to the Modeling of Hydrosystems.* Springer Verlag, 1997.

[26] R. Helmig, C. Braun, and M. Emmert. *MUFTE – A numerical model for the simulation of multiphase flow processes in porous and fractured–porous media – nonisothermal twophase–twocomponent module.* Institut f"ur Wasserbau, Universit"at Stuttgart, 1996. Programmdokumentation.

[27] R. Helmig, H. Class, H. Huber, H. Sheta, R. Ewing, R. Hinkelmann, H. Jakobs, and P. Bastian. Architecture of the Modular Program System MUFTE_UG for Simulating Multiphase Flow and Transport Processes in Heterogeneous Porous Media. *Mathematische Geologie*, 2, 1998.

[28] International Formulation Committee. A formulation of the thermodynamic properties of ordinary water substance. Technical report, IFC Sekretariat, D"usseldorf, Germany, 1967.

[29] B.H. Kueper and E.O. Frind. Numerical Modelling of Multiphase/Multicomponent Flow and Transport in Porous Media: An Overview. Paper, presented at Int. Assoc. Hydrogeol. Conf. on Subsurface Contamination by immiscible Fluids , Calgary, Alberta, 1990.

[30] R.J. Lenhard. Scaling fluid content–pressure relations of different fluid systems in porous media. In H.J. Morel-Seytoux, editor, *14th Annual American Geophysical Union Hydrology Days*, volume CA:223–235, Atherton, 1994. Hydrology Days Publ.

[31] M.C. Leverett. *Capillary Behavior in Porous Solids*, volume 142. AIME Transactions, 1941.

[32] D.R. Lide. *CRC Handbook of Chemistry and Physics.* CRC Press, Boca Raton, 1995.

[33] B.B. Looney and R.W. Falta. *Vadose Zone.* Battelle Press, Columbus, OH, 2000.

[34] S. Panday, P.A. Forsyth, R.W. Falta, Y. Wu, and P.S. Huyakorn. Considerations for robust compositional simulations of subsurface nonaqueous phase liquid contamination and remediation. *Water Resour. Res.*, 31(5):1273–1289, 1995.

[35] J.C. Parker and R.J. Lenhard. A Model for Hysteretic Constitutive Relations Governing Multiphase Flow, 1. Saturation–Pressure Relations. *Water Resour. Res.*, 23(12):2187–2196, 1987.

[36] J.C. Parker, R.J. Lenhard, and T. Kuppusami. A Parametric Model for Constitutive Properties Governing Multiphase Flow in Porous Media. *Water Resour. Res.*, 23(4):618–624, 1987.

[37] K. Pruess. TOUGH User's Guide. Technical report, Lawrence Berkeley Laboratory, University of California, 1987. LBL-20700.

[38] K. Pruess. TOUGH2 - A General–Purpose Numerical Simulator for Multiphase Fluid and Heat Flow. Technical report, Lawrence Berkeley Laboratory, University of California, 1991. LBL-29400.

[39] K. Pruess and T.N. Narasimhan. On fluid reserves and the production of superheated steam from fractured, vapor-dominated geothermal reservoirs. *Journal of Geophysical Research*, 87(B11):9329–9339, 1982.

[40] R.C. Reid, J.M. Prausnitz, and B.E. Poling. *The Properties of Gases and Liquids*. McGraw-Hill, Inc., 1987.

[41] H.Y. She and B.E. Sleep. The effect of temperature on capillary pressure-saturation relationships for air-water and perchloroethylene-water systems. *Water Resour. Res.*, 34(10):2587–2597, 1998.

[42] K.S. Udell and J.S. Fitch, editors. *Heat and mass transfer in capillary porous media considering evaporation, condensation and non-condensible gas effects*, Denver, CO, August 1985. Paper presented at 23rd ASME/AIChE National Heat Transfer Conference.

[43] K.S. Udell and L.D. Stewart. Field study of in-situ steam injection and vacuum extraction for recovery of volatile organic solvents. Technical Report UCB-SEEHRL-89-2, University of California, Berkeley, 1989.

[44] M.Th. van Genuchten. A closed-form equation for predicting the hydraulic conductivity of unsaturated soils. *Soil Sci. Soc. Am. J.*, 44:892–898, 1980.